Extracellular matrix macro-assembly dynamics in early vertebrate embryos

Andras Czirok,[1,2,*] Evan A. Zamir,[1] Michael B. Filla,[1] Charles D. Little[1] and Brenda J. Rongish[1]

[1] Dept. of Anatomy and Cell Biology, University of Kansas Medical Center. Kansas City, KS 66160.

[2] Dept. of Biological Physics, Eotvos University. Budapest, 1117 Hungary.

*Correspondence: aczirok@kumc.edu, phone: (+913)-588-1857, fax: (+913)-588-2710

Running Head: ECM macro-assembly

Current Topics in Developmental Biology, in press.

Contents

Abstract 3

I Introduction 4

II Localization and function of select ECM components 6

II.1 Fibronectin 6

II.2 Fibrillin-2 8

II.3 Co-localization 9

III ECM position fate 10

IV ECM displacement mapping 11

IV.1 Correlated motion 11

IV.2 Displacement decomposition 12

IV.3 Particle image velocimetry 13

V The tissue motion component of ECM displacement 14

VI Local ECM rearrangements 15

VI.1 Magnitude and diversity 15

VI.2 Filament assembly 16

VII Conclusions 16

References 18

Figure captions 28

Abstract

This review focuses on the *in vivo* macro-assembly dynamics of fibronectin and fibrillin-2 – two prominent ECM components, present in vertebrate embryos at the earliest stages of development. The ECM is an inherently dynamic structure with a well defined position fate: ECM filaments are not only anchored to and move with established tissue boundaries, but are repositioned prior to the formation of new anatomical features. We distinguish two ECM filament relocation processes – each operating on different length scales. First, ECM filaments are moved by large-scale tissue motion, which rearranges major organ primordia within the embryo. The second type of motion, on the scale of the individual ECM filaments, are driven by local motility and protrusive activity of nearby cells. The motion decomposition is made practically possible by recent advances in microscopy and high resolution particle image velocimetry algorithms. We demonstrate that both kinds of motion contribute substantially to the establishment of normal ECM structure, and both must be taken into account when attempting to understand ECM macro-assembly during embryonic morphogenesis. The tissue-scale motion changes the local amount (density) and the tissue-level structure (e.g., orientation) of ECM fibers. Local reorganization includes filament assembly and the segregation of ECM into specific patterns. Local reorganization takes place most actively at Hensen's node and around the primitive streak. These regions are also sites of active cell migration, where fibrillin-2 and fibronectin are often co-localized in ECM globules, and new fibrillin-2 foci are deposited. During filament assembly, the globular patches of ECM are joined into larger linear structures in a hierarchical process: increasingly larger structures are created by the aggregation of smaller units. A future understanding of ECM assembly thus requires the study of the complex interactions between biochemical assembly steps, local cell action and tissue motion.

I Introduction

There is a rich history of studies on extracellular matrix (ECM) biology during embryogenesis, starting with the ground breaking studies of Rudnick, Grobstein, Hay and Gross (Rudnick, 1933; Grobstein, 1954; Gross, 1974; Hay, 1982). These pioneering studies established the critical role of ECM in development. The discovery and characterization of the integrin family of ECM receptors (Pytela et al., 1985; Hynes, 1987) was another major breakthrough in the field, triggering an avalanche of research studies. The basic molecular intricacies of ECM synthesis, secretion, cytoskeletal interactions and assembly have now been described. It is established that the ECM provides adhesive substrates and signals for cell migration and differentiation (Hay, 1990; George et al., 1993), modulates the availability of growth factors (Charbonneau et al., 2004; Dallas et al., 2005) and contributes to the mechanical integrity of tissues (Sherratt et al., 2003; Kadler, 2004). To fit these pieces of information into an understanding of how the ECM functions *in vivo* during development and in mature tissues remains a daunting task – requiring further research into the relationships between the various organization levels that span from molecules to organs. Due to the very nature of the problem, the required approaches are multi-disciplinary, incorporating anatomical, biochemical, physical and tissue engineering concepts.

The three dimensional (3D) organization of the ECM can be as crucial as its molecular composition in determining its developmental functions. Cell-ECM contacts strongly depend on how the ECM is presented to cell surface receptors, whether it is immobilized, planar or three dimensional (Zamir et al., 1999; Cukierman et al., 2001). ECM organization also strongly influences cell shape

and motility (Tomasek et al., 1982; Petroll and Ma, 2003): Fibroblasts (Stoplak and Harris, 1982; Dickinson et al., 1994), endothelial cells (Vernon et al., 1995), and neurons (Dubey et al., 2001), are all known to preferentially follow oriented fibers. At the tissue level of organization, mechanical properties, such as anisotropy or load bearing capacity, are determined by 3D ECM structure (Barocas and Tranquillo, 1997; Olsen et al., 1999).

ECM structure, as a physical entity, is molded by mechanical stress (Keller et al., 2003). The most relevant source of mechanical stress is cellular traction force (Stoplak and Harris, 1982; Oliver et al., 1995), which was demonstrated to reorganize collagen filaments *in vitro* (Petroll and Ma, 2003; Friedl and Wolf, 2003). The mechanically-driven ECM reorganization is often not reversible due to modifications in molecular configuration, which in turn enable chemical crosslinking or proteolysis (Wolf and Friedl, 2005). The best understood example of such a reorganization, at the molecular level, is that of fibronectin, where traction forces are needed to change the conformation of individual fibronectin molecules and expose a cryptic binding site (Zhong et al., 1998; Baneyx et al., 2001). Thus macro-assembly, the 3D (and possibly tissue-scale) ECM organization, is not only the sum of all biochemical reactions forming ECM protein complexes, but also involves tissue mechanics and sophisticated cell behavior (Hay, 1982).

While the importance of data obtained from cell culture studies cannot be overestimated, the most commonly used culture methods have inherent limitations in the study of ECM dynamics. Attachment of the ECM to a rigid substrate creates mechanical boundary conditions which restrict substantial deformation. Thus, the traction stress exerted by a cell affects only the ECM in the immediate vicinity. Embryonic tissues, in contrast, undergo large deformations during organogenesis. These tissue motions are responses to intrinsic mechanical stresses, generated by a concerted action of large cell collectives, many of which are located at distant sites in the embryo (Trinkaus,

1984; Cowin, 2000; Keller et al., 2003). Thus, during morphogenesis, the ECM is expected to exhibit far more substantial rearrangements than those observed in cell cultures. Moreover, *in vivo* ECM macro-assembly can be affected by remote morphological events mediated through long-range mechanical stress fields, extending over hundreds of cell diameters. To tackle these challenges, quantitative experimental data on ECM behavior are needed. Such data would facilitate our understanding and allow the formulation and testing of sophisticated mathematical models with quantitative prediction power.

Here we review and report on the macro-assembly dynamics of fibronectin and fibrillin-2 – two prominent, ubiquitous ECM components, present in vertebrate embryos at the earliest (pre-gastrulation) stages of development. We demonstrate that at gastrulation and neurulation stages the ECM is far from a static structure: it moves, rearranges and its components have well defined position fates.

II Localization and function of select ECM components

[FIGURE 1]

II.1 Fibronectin

Fibronectin is one of the earliest ECM proteins to be deposited in the embryo. As Fig. 1 demonstrates, fibronectin is present along the basal surface of the ectoderm and endoderm in gastrulating avian embryos, and in filaments around Hensen's node (Krotoski et al., 1986). Studies of amphibian embryos established that fibronectin is a major component of the ECM assembled along the blastocoel roof and other tissue interfaces (Lee et al., 1984; Danker et al., 1993). In fact, ev-

ery mesodermal cell at late gastrula and early neurula stages appears to be in direct contact with a fibronectin-rich filamentous matrix (Davidson et al., 2004). Recently, Davidson et al. (2004) demonstrated that fibronectin is deposited rather rapidly at the mesoderm-endoderm interface during the time when the endoderm involutes over the blastopore lip. The same study also showed that fibronectin-rich ECM is created, removed and subsequently reestablished during Xenopus development: Fibrils are cleared from the dorsal and ventral faces of the notochord, and at the same time appear medially, at the neural/somitic mesoderm boundary. As the neural plate thickens, fibronectin fibrils are reestablished between the dorsal notochord surface. The deposition of fibronectin fibers takes place at tissue boundaries, especially at sites of shear motion between tissues.

Fibronectin is mainly known to promote cell adhesion and migration. Fibronectin was shown to be necessary for ingressed mesoblast cell migration away from the primitive streak (Harrisson et al., 1993), and for the extension of the mesendoderm and radial intercalation in Xenopus embryos (Davidson et al., 2002; Marsden and DeSimone, 2001). Fibronectin fibrils lining the Xenopus animal cap ectoderm (Lee et al., 1984; Nakatsuji et al., 1985) are used as a substrate for mesendoderm migration (Darribere et al., 1988; Winklbauer and Keller, 1996). Fibronectin null mutations in mice are embryonic lethal, with mesodermal defects and failed notochord or somite formation (George et al., 1993). In addition to its role in promoting cell migration, several *in vitro* studies have suggested that fibronectin is required during the assembly of multiple ECM proteins, including collagen types I and III (McDonald et al., 1982; Velling et al., 2002), fibulin (Godyna et al., 1995; Roman and McDonald, 1993), fibrinogen (Pereira et al., 2002), thrombospondin (Sottile and Hocking, 2002) and LTBP1 (Dallas et al., 2005).

II.2 Fibrillin-2

The fibrillin family of ECM proteins are constituents of connective tissue microfibrils (Sakai et al., 1986; Zhang et al., 1994; Corson et al., 2004). Fibrillin-2 is observed in the avian embryo before gastrulation in the form of slender filaments marking the future anterior-posterior axis (Wunsch et al., 1994). During gastrulation, fibrillin-2 continues to display a remarkable pattern widely distributed in association with the mesoderm (Rongish et al., 1998; Visconti et al., 2003) (Fig. 1): a meshwork encases the notochord and fibrillin-2 cables connect the anterior intestinal portal to the somites. Most notable are the bundles of fibers that run parallel to the embryonic axis. The cranial portion of these bundles encloses the somites, while caudally the cables extend more than 200 μm into the segmental plate mesoderm and approach Hensen's node. Caudal to the node, fibrillin-2 exhibits a different pattern, which consists of punctate, unconnected fluorescent foci. In Xenopus embryos, a fibrillin homolog (XF) is expressed from blastula stages onward. At early gastrula stages XF expression is restricted to the recently involuted mesoderm and the XF protein is observed as two stripes flanking the presumptive notochord. After neural tube closure, XF demarcates the notochord and the intersomitic clefts (Dr. Paul Skoglund, Univ. of Virginia, VA, personal communication).

The importance of the fibrillin family of ECM proteins to the structural and functional properties of connective tissues is demonstrated by the fact that mutations in the human fibrillin genes result in heritable disorders, with patients manifesting ocular, skeletal, and cardiovascular abnormalities (Dietz et al., 1994). In accord, fibrillin-deficient mouse models demonstrated that the absence of normal levels of either fibrillin-1 or 2 protein is incompatible with the proper function of mature elastic fibers (Arteaga-Solis et al., 2001; Pereira et al., 1997, 1999). Deficiency in both fibrillin-1 and 2 was found to be compatible with gastrulation of mouse embryos, but the embryos

died before birth (Dr. Luca Carta, Hospital for Special Surgery, NY, personal communication). In contrast, exogenous expression of a truncated fibrillin in the presumptive dorsal mesoderm of gastrulation stage frog embryos disturbed endogenous fibrillin localization and blocked gastrulation (Skoglund, 1996).

II.3 Co-localization

As Fig. 1 demonstrates, the general organization of both fibronectin and fibrillin-2 is surprisingly similar. Both proteins are associated with ECM filaments throughout the lateral embryo, and exhibit a punctate pattern at Hensen's node and in the caudal part of the embryo (boxed region B). Both accumulate at the dorsal and ventral surface of the mesodermal germ layer, in filaments which traverse the mesoderm, and encase the notochord and the somites. While fibronectin and fibrillin-2 distribution is similar, confocal sections show that in general, these molecules are not extensively co-localized. One significant exception is the caudal embryo, where fibrillin-2 immunoreactive filaments often appear decorated with fibronectin foci at the resolution of confocal light microscopy (Fig. 1g and 1h). Although fibronectin is not an elastic fiber constituent, their association is not uncommon (Goldfisher et al., 1985; Latif et al., 2005). While there is no biochemical evidence for direct binding between fibrillins and fibronectin under physiological conditions, these two ECM components may interact by both binding to versicans (Wu et al., 2005), fibulins (Timpl et al., 2003), matrilin-2 (Piecha et al., 2002) and LTBP1 (Dallas et al., 2000).

III ECM position fate

Recent advances in optical microscopy and molecular technologies allow the *in situ* visualization of morphogenic processes with micrometer scale resolution (Lansford et al., 2001; Kulesa, 2004; Friedl, 2004). The same technologies also made possible the study of supramolecular, cellular- and tissue-scale ECM assembly, both in cell cultures and *in vivo* (Ohashi et al., 1999; Czirok et al., 2004; Davidson et al., 2004; Kozel et al., 2006; Sivakumar et al., 2006).

[FIGURE 2]

Dynamic imaging studies in avian embryos reveal that fibronectin and fibrillin-2 containing ECM filaments are substantially displaced during development (see Fig. 2, and Czirok et al. (2004); Filla et al. (2004)). During this process ECM filaments typically retain their characteristic shape and connectivity with adjacent filaments. Position changes, therefore, are interpreted as physical displacements of intact objects rather than as a process involving filament disassembly and reassembly. Based on this approach, one can determine the position fate of ECM filaments – in a manner analogous to cell fate mapping. This fate is not trivial: ECM filaments are not only anchored to and move with established tissue boundaries, but are rearranged and repositioned prior to the formation of new anatomical features. An example is presented in Fig. 2, where fibrillin-2 filaments associated with the segmental plate mesoderm are assembled into parallel cables at the position of future somites. The demarcation between the axial cables and the less organized lateral meshwork of fibrillin-2 is fuzzy and does not coincide with preexisting anatomical structures. Once somites form, the axial cables become part of the dense ECM meshwork that encloses and connects all somites. In fact, pre-existing ECM filaments with long lifetimes are used in a similar manner during the formation of other early embryonic structures including the foregut, heart or

blood vessels (unpublished data). At present, the relationship between cell and ECM fate maps remains an open problem – in the concluding section we present conjectures on this relationship after further analysis of *in situ* ECM dynamics.

IV ECM displacement mapping

[FIGURE 3]

ECM formation is best studied in caudal regions of early avian embryos, where tissue geometry is relatively uncomplicated. To ensure the simultaneous visualization of all ECM filaments within this area, images are taken in multiple focal planes. To characterize the dynamics of ECM rearrangements, filament segments can be followed through the image sequence, their position registered relative to some stable anatomical reference points (like the intersomitic clefts) and their displacements calculated (Czirok et al., 2004). Although tracking procedures can be performed in 3D, due to the large depth of field of the microscope objective, the resolution along the vertical (z) direction is rather limited. In fact, in the wide-field epifluorescence microscopy setup, the optical depth of field is comparable to the specimen thickness. Therefore, our studies analyze the two-dimensional (x-y) projections of the physical (3D) ECM displacements.

[FIGURE 4]

IV.1 Correlated motion

The analysis of image sequences reveal that ECM motion is ordered in space since displacements of adjacent filaments are similar: Changes in the relative position of nearby filaments are far smaller than the observed displacement of the ECM composite (Fig. 3a). To visualize temporal changes

in ECM motion, fluorescence intensity profiles are calculated along a line parallel to the motion of the filaments. The resulting intensity profiles are shown in Fig. 4c for each frame in the image sequence. The intersection between ECM filaments and the selected line is marked by intensity peaks. As filaments move, the location of the intensity peaks shifts, resulting in continuous curves on the spatio-temporal intensity plot. The smoothness and overall similarity of the curves in Fig. 4c indicate a slowly changing, correlated and persistent motion where displacements tend to continue over many hours in a similar fashion. Thus, ECM filaments seem to be embedded in a moving and continuous mechanical medium, rather than existing as free-moving or quickly disconnecting and reconnecting polymers.

Images analyzed in Fig. 3 and in (Czirok et al., 2004) depict every fluorescence-tagged ECM filament, irrespective of their dorsal-ventral location. Because of the absence of ECM filament populations displaying markedly different displacements, we can exclude the possibility of large dorsal-ventral differences in motion. Thus, ECM filaments located either in the mesoderm, at the mesoderm-endoderm or mesoderm-ectoderm boundaries show approximately the same displacements.

IV.2 Displacement decomposition

In addition to the above data, we know that although the motion of ECM filaments may be similar, there must be differences which eventually result in distinct patterns along the dorsal-ventral axis or between different kinds of ECM proteins. It is thus reasonable to distinguish two ECM filament relocation processes – each operating on different length scales. First, ECM filaments are expected to be moved by large-scale tissue motion, which rearranges major organ primordia within the embryo. A second type of motion, on the scale of the individual ECM filaments, could be driven

by local motility and protrusive activity of the nearby cells. Although any kind of motion can be arbitrarily divided into two scales, the model posed here predicts that the large-scale motion component is the same for all ECM components, while the local rearrangements must be ECM component specific, to account for the observed differences in the various distribution patterns. Moreover, the local action of the cells is expected to operate on shorter characteristic time scales (minutes) than global tissue movements (hours). As we will learn from the data below, both kinds of motion contribute substantially to normal ECM structure, and both must be taken into account when attempting to understand ECM macro-assembly during embryonic morphogenesis.

IV.3 Particle image velocimetry

The decomposition of ECM movements into two processes was made possible by adopting high resolution (sub-pixel) particle image velocimetry (PIV) techniques (Zamir et al., 2005) in tracing the filaments. In the PIV analysis of "optical flow", image details are traced through the image sequence without the need for segmentation and recognition of distinct objects. As the red arrows in Fig. 3b demonstrate, a two-step predictor-corrector PIV algorithm approximates the manual tracking very closely. The extraction of the tissue motion component, i.e., the motion of a mechanical continuum, can be done by local averaging of the individual ECM filament displacements (Czirok et al., 2004) or by spline smoothing of the results of a coarser PIV calculation (Zamir et al., 2005). Both approaches rely on the presence of local spatial and temporal correlations, i.e., on the fact that adjacent ECM filaments continue to move similarly. The second, local component of the motion is obtained as the difference of the actual displacements (tracked either manually or with high resolution PIV) and the tissue motion component (Fig. 4d).

V The tissue motion component of ECM displacement

[FIGURE 5]

[FIGURE 6]

The overall direction of ECM motion is highly reproducible across embryos Czirok et al. (2004). Moreover, as Fig. 5 demonstrates, the tissue component of the motion is the same for both fibronectin and fibrillin-2, and is best described as two, counter-rotating vortices on each side of Hensen's node (Fig. 6). This displacement pattern appears to move with the node, as it regresses caudally over time.

[FIGURE 7]

The displacement field presented in Fig. 6 has two important implications for morphogenesis: it changes both the local amount (density) and the tissue-level structure of the ECM. Calculation of the divergence of the displacement field reveals how the motion changes the amount of labeled ECM components present within a certain area. As Fig. 7a demonstrates, ECM is condensed around the site of somitogenesis. In contrast, in the caudal embryo labeled ECM filaments are scattered within an increasing area, so their density decreases. Interestingly, this region of expansion coincides with the deposition and assembly of new, and thus unlabeled, ECM filaments (unpublished data) – a process that may counterbalance the observed local decreased density of labeled filaments. The observed tissue movements can result in ECM density changes of up to 10%/hour, and thus yield a substantial cumulative compression of the ECM over the duration of gastrulation (Zamir et al., 2005). A mathematical decomposition (Abraham et al., 1988) reveals the deformation of the tissue motion component (Fig. 7b). The deformation is maximal between Hensen's node and the somitogenesis front, and appears to play a major role in the transformation

of the loose meshwork, characteristic for the segmental-plate associated ECM, into anisotropic, axial cables.

VI Local ECM rearrangements

[FIGURE 8]

VI.1 Magnitude and diversity

As described in section IV, local ECM rearrangements are obtained after subtracting the tissue motion component from the displacement data. This local component of ECM displacement, depicted in Fig. 4d, changes quickly in space and time. As Fig. 5 demonstrates, local rearrangements are different for fibronectin and fibrillin-2 and have magnitudes typically five times smaller than that of the tissue motion component. As local ECM rearrangement is presumably correlated with cell motility and protrusive activity, the magnitude of the local component is an approximate measure of the ECM remodeling activity of cells. Fig. 8 shows the distribution of the magnitude of the local ECM rearrangement within the caudal embryo. Most active local ECM reorganization takes place at Hensen's node and around the primitive streak. In this "active" region (red area in Fig. 8) the ECM does not form an interconnected network, fibrillin-2 and fibronectin are often co-localized (Fig. 1) and new fibrillin-2 foci are deposited (unpublished results). The "active" region also coincides with the location where mesodermal cells migrate intensively after ingression (Schoenwolf et al., 1992; Psychoyos and Stern, 1996).

VI.2 Filament assembly

[FIGURE 9]

Filament assembly, a particularly interesting reorganization process, also takes place in the caudal embryo. Globular patches of immunofluorescence are joined into larger linear structures as shown in Fig. 9. Closer analysis reveals that the process appears to be hierarchical: increasingly larger structures are created by the aggregation of smaller units. Throughout the assembly process, participating ECM filaments appear to consist of both fibronectin and fibrillin-2; thus filaments are "born" as composite structures. While a set of globules and short filaments is often observed to assume a linear pattern, in our pulse-chase experiments some fibers do not appear to be fully connected. Presumably, newly produced or different and thus unlabeled ECM proteins fill in the gaps, but are not visualized.

The dynamics of macro-assembly of fibronectin (Ohashi et al., 2002), LTBP (Sivakumar et al., 2006) and elastin (Kozel et al., 2006; Czirok et al., 2006) filaments was recently investigated in various cell culture models. In case of densely populated cell cultures these studies showed that the ECM is assembled first in distinct globules on the cell surface. Subsequently, through the motion of several adjacent cells, these ECM foci are organized into progressively larger filaments. In the case of elastin, ECM filaments were shown to aggregate in a hierarchical fashion similar to Fig. 9 (Czirok et al., 2006).

VII Conclusions

The present data inevitably raise questions about possible relationships between ECM motion and the features of mesodermal cell migration (Schoenwolf et al., 1992; Psychoyos and Stern, 1996).

We expect a similar approach to be applicable to cell motion and cell fate mapping. Using the same arguments as those presented in section IV, cell displacements can also be decomposed into a tissue and a local motion component – the latter reflecting the autonomous motion of individual cells relative to the tissue (Sepich et al., 2005). We predict that the tissue motion component of the mesodermal cells and mesoderm-associated ECM are the same. Moreover, as tissue motion can be a response to forces exerted by distant cell collectives, we speculate that the remarkable vortices of DiI labeled cells reported recently by Yang et al. (2002) and Cui et al. (2005) could be explained as a tissue mechanical phenomenon whereby propulsion is generated by forces exerted around the notochord, foregut and in the area opaca.

This review demonstrates that ECM structure *in vivo* is formed through complex interactions including biochemical assembly steps, local cell behavior and tissue motion. We hope we have conveyed that a future understanding of *in vivo* ECM formation, as well as its function, will require the synthesis of a vast spectrum of studies ranging from determining protein conformations to computer modeling of embryonic tissue movements during organogenesis.

Acknowledgements

We are grateful to Tracey Cheuvront and Alan Petersen for their technical expertise, and to Cheng Cui for fruitful discussions. The help of Elizabeth Petroske with confocal imaging is greatly appreciated. This work was supported by the G Harold and Leila Y Mathers Charitable Foundation (to C.D.L.), the NIH (R01 HL68855 to C.D.L., R01 HL73700 to B.J.R.), the American Heart Association (Scientist Development Grant 0535245N to A.C, Heartland Affiliate postdoctoral fellowship to E.A.Z) and the Hungarian Research Fund (OTKA T047055, to A.C.). The JB3 and B3D6 antibodies were obtained from the Developmental Studies Hybridoma Bank at the Univ. of Iowa.

References

Abraham, R., Marsden, J., Ratiu, T., 1988. Manifolds, tensor analysis and applications. Springer, Berlin.

Arteaga-Solis, E., Gayraud, B., Lee, S., Shum, L., Sakai, L., Ramirez, F., 2001. Regulation of limb patterning by extracellular microfibrils. J Cell Biol. 154, 275–281.

Baneyx, G., Baugh, L., Vogel, V., 2001. Coexisting conformations of fibronectin in cell culture imaged using fluorescence resonance energy transfer. Proc Natl Acad Sci U S A 98, 14464–8.

Barocas, V., Tranquillo, R., 1997. An anisotropic biphasic theory of tissue-equivalent mechanics: the interplay among cell traction, fibrillar network deformation, fibril alignment, and cell contact guidance. J Biomech. Eng. 119(2), 137–145.

Charbonneau, N. L., Ono, R. N., Corson, G. M., Keene, D. R., Sakai, L. Y., 2004. Fine tuning of growth factor signals depends on fibrillin microfibril networks. Birth Defects Res C Embryo Today 72, 37–50.

Corson, G., Charbonneau, N., Keene, D., Sakai, L., 2004. Differential expression of fibrillin-3 adds to microfibril variety in human and avian, but not rodent, connective tissues. Genomics 83, 461–72.

Cowin, S., 2000. How is a tissue built? J Biomech Eng. 122, 553–69.

Cui, C., Yang, X., Chuai, M., Glazier, J. A., Weijer, C. J., 2005. Analysis of tissue flow patterns during primitive streak formation in the chick embryo. Dev Biol. 284, 37–47.

Cukierman, E., Pankov, R., Stevens, D. R., Yamada, K. M., 2001. Taking cell-matrix adhesions to the third dimension. Science 294, 1708–12.

Czirok, A., Rongish, B. J., Little, C. D., 2004. Extracellular matrix dynamics during vertebrate axis formation. Dev Biol 268, 111–22.

Czirok, A., Zach, J., KOzel, B., Mecham, R., Davis, E., Rongish, B., 2006. Elastic fiber macro-assembly is a hierarchical, cell motion-mediated process. J Cell. Physiol. xxx, xxx–xx.

Dallas, S. L., Keene, D. R., Bruder, S. P., Saharinen, J., Sakai, L. Y., Mundy, G. R., Bonewald, L. F., 2000. Role of the latent transforming growth factor beta binding protein 1 in fibrillin-containing microfibrils in bone cells in vitro and in vivo. J Bone Miner Res 15, 68–81.

Dallas, S. L., Sivakumar, P., Jones, C. J. P., Chen, Q., Peters, D. M., Mosher, D. F., Humphries, M. J., Kielty, C. M., 2005. Fibronectin regulates latent transforming growth factor-beta (tgf beta) by controlling matrix assembly of latent tgf beta-binding protein-1. J Biol Chem 280, 18871–80.

Danker, K., Hacke, H., Ramos, J., DeSimone, D., Wedlich, D., 1993. V(+)-fibronectin expression and localization prior to gastrulation in xenopus laevis embryos. Mech Dev 44, 155–65.

Darribere, T., Yamada, K. M., Johnson, K. E., Boucaut, J. C., 1988. The 140-kda fibronectin receptor complex is required for mesodermal cell adhesion during gastrulation in the amphibian pleurodeles waltlii. Dev Biol 126, 182–94.

Davidson, L. A., Hoffstrom, B. G., Keller, R., DeSimone, D. W., 2002. Mesendoderm extension

and mantle closure in xenopus laevis gastrulation: combined roles for integrin alpha(5)beta(1), fibronectin, and tissue geometry. Dev Biol 242, 109–29.

Davidson, L. A., Keller, R., DeSimone, D. W., 2004. Assembly and remodeling of the fibrillar fibronectin extracellular matrix during gastrulation and neurulation in xenopus laevis. Dev Dyn 231, 888–95.

Dickinson, R., Guido, S., Tranquillo, R., 1994. Biased cell migration of fibroblasts exhibiting contact guidance in oriented collagen gels. Ann. Biomed. Eng. 22(4), 342–356.

Dietz, H., Ramirez, F., Sakai, L., 1994. Marfan syndrome and other microfibrillar diseases. Adv. Hum. Genet. 22, 153–86.

Dubey, N., Letourneau, P., Tranquillo, R., 2001. Neuronal contact guidance in magnetically aligned fibrin gels: effect of variation in gel mechano-structural properties. Biomaterials 22(10), 1065–1075.

Filla, M. B., Czirok, A., Zamir, E. A., Little, C. D., Cheuvront, T. J., Rongish, B. J., 2004. Dynamic imaging of cell, extracellular matrix, and tissue movements during avian vertebral axis patterning. Birth Defects Res C Embryo Today 72, 267–76.

Friedl, P., 2004. Dynamic imaging of cellular interactions with extracellular matrix. Histochem Cell Biol 122, 183–90.

Friedl, P., Wolf, K., 2003. Tumour-cell invasion and migration: diversity and escape mechanisms. Nat Rev Cancer , 362–74.

George, E. L., Georges-Labouesse, E. N., Patel-King, R. S., Rayburn, H., Hynes, R. O., 1993. De-

fects in mesoderm, neural tube and vascular development in mouse embryos lacking fibronectin. Development 119, 1079–91.

Godyna, S., Mann, D. M., Argraves, W. S., 1995. A quantitative analysis of the incorporation of fibulin-1 into extracellular matrix indicates that fibronectin assembly is required. Matrix Biol 14, 467–77.

Goldfisher, S., Coltoff-Schiller, B., Goldfisher, M., 1985. Microfibrils, elastic anchoring components of the extracellular matrix, are associated with fibronectin in the zonule of zinn and aorta. Tissue Cell 17, 441–50.

Grobstein, C., 1954. Tissue interaction in morphogenesis of mouse embryonic rudiments in vitro. In: Rudnick, G. (Ed.) Aspects of synthesis and order in growth, Princeton Univ. Press, Princeton, NJ, pp. 233–256.

Gross, J., 1974. Collagen biology: structure, degradation and disease. Harvey Lectures 68, 351–432.

Hamburger, V., Hamilton, H., 1951. A series of normal stages in the development of the chick embryo. J. Morphol. 88, 49 – 92.

Harrisson, F., Van Nassauw, L., Van Hoof, J., Foidart, J. M., 1993. Microinjection of antifibronectin antibodies in the chicken blastoderm: inhibition of mesoblast cell migration but not of cell ingression at the primitive streak. Anat Rec 236, 685–96.

Hay, E. (Ed.) , 1982. Cell Biology of Extracellular Matrix. Plenum Press, New York.

Hay, E. D., 1990. Role of cell-matrix contacts in cell migration and epithelial-mesenchymal transformation. Cell Differ Dev 32, 367–75.

Hynes, R. O., 1987. Integrins: a family of cell surface receptors. Cell 48, 549–54.

Kadler, K., 2004. Matrix loading: assembly of extracellular matrix collagen fibrils during embryogenesis. Birth Defects Res C Embryo Today 72, 1–11.

Keller, R., Davidson, L. A., Shook, D. R., 2003. How we are shaped: the biomechanics of gastrulation. Differentiation 71, 171–205.

Kozel, B., Rongish, B., Czirok, A., Zach, J., Little, C., Davis, E., Knutsen, E., Wagenseil, J., Levy, M., Mecham, R., 2006. Elastic fiber formation: a dynamic view of extracellular matrix assembly using timer reporters. J Cell. Physiol. xxx, xxx–xx.

Krotoski, D. M., Domingo, C., Bronner-Fraser, M., 1986. Distribution of a putative cell surface receptor for fibronectin and laminin in the avian embryo. J Cell Biol 103, 1061–71.

Kulesa, P. M., 2004. Developmental imaging: Insights into the avian embryo. Birth Defects Res C Embryo Today 72, 260–6.

Lansford, R., Bearman, G., Fraser, S. E., 2001. Resolution of multiple green fluorescent protein color variants and dyes using two-photon microscopy and imaging spectroscopy. J Biomed Opt , 311–8.

Latif, N., Sarathchandra, P., Taylor, P., Antoniw, J., Yacoub, M., 2005. Localization and pattern of expression of extracellular matrix components in human heart valves. J Heart Valve Dis. 14, 218–27.

Lee, G., Hynes, R., Kirschner, M., 1984. Temporal and spatial regulation of fibronectin in early xenopus development. Cell 36, 729–40.

Marsden, M., DeSimone, D. W., 2001. Regulation of cell polarity, radial intercalation and epiboly in xenopus: novel roles for integrin and fibronectin. Development 128, 3635–47.

McDonald, J., Kellet, D., Broekelmann, T., 1982. Role of fibronectin in collagen deposition. J. Cell Biol. 92, 485 – 92.

Nakatsuji, N., Smolira, M. A., Wylie, C. C., 1985. Fibronectin visualized by scanning electron microscopy immunocytochemistry on the substratum for cell migration in xenopus laevis gastrulae. Dev Biol 107, 264–8.

Ohashi, T., Kiehart, D. P., Erickson, H. P., 1999. Dynamics and elasticity of the fibronectin matrix in living cell culture visualized by fibronectin-green fluorescent protein. Proc Natl Acad Sci U S A 96, 2153–8.

Ohashi, T., Kiehart, D. P., Erickson, H. P., 2002. Dual labeling of the fibronectin matrix and actin cytoskeleton with green fluorescent protein variants. J Cell Sci 115, 1221–9.

Oliver, T., Dembo, M., Jacobson, K., 1995. Traction forces in locomoting cells. Cell Motil. Cytoskeleton 31(3), 225–40.

Olsen, L., Maini, P., Sherratt, J., Dallon, J., 1999. Mathematical modelling of anisotropy in fibrous connective tissue. Mathematical Biosciences 158, 145–170.

Pereira, L., Andrikopoulos, K., Tian, J., Lee, S., Keene, D., Ono, R., Reinhardt, D., Sakai, L., Biery, N., Bunton, T., Dietz, H., Ramirez, F., 1997. Targeting of the gene encoding fibrillin-1 recapitulates the vascular aspect of Marfan syndrome. Nat. Genet. 17, 218–222.

Pereira, L., Lee, S., Gayraud, B., Andrikopoulos, K., Shapiro, S., Bunton, T., Biery, N., Dietz, H.,

Sakai, L., Ramirez, F., 1999. Pathogenic sequence for aneurysm revealed in mice underexpressing fibrillin-1. Proc. Natl. Acad. Sci. 96, 3819–3823.

Pereira, M., Rybarczyk, B. J., Odrljin, T. M., Hocking, D. C., Sottile, J., Simpson-Haidaris, P. J., 2002. The incorporation of fibrinogen into extracellular matrix is dependent on active assembly of a fibronectin matrix. J Cell Sci 115, 609–17.

Petroll, W. M., Ma, L., 2003. Direct, dynamic assessment of cell-matrix interactions inside fibrillar collagen lattices. Cell Motil Cytoskeleton 55, 254–64.

Piecha, D., Wiberg, C., Morgelin, M., Reinhardt, D. P., Deak, F., Maurer, P., Paulsson, M., 2002. Matrilin-2 interacts with itself and with other extracellular matrix proteins. Biochem J 367, 715–21.

Psychoyos, D., Stern, C., 1996. Fates and migratory routes of primitive streak cells in the chick embryo. Development 122(5), 1523–34.

Pytela, R., Pierschbacher, M. D., Ruoslahti, E., 1985. Identification and isolation of a 140 kd cell surface glycoprotein with properties expected of a fibronectin receptor. Cell 40, 191–8.

Roman, J., McDonald, J. A., 1993. Fibulin's organization into the extracellular matrix of fetal lung fibroblasts is dependent on fibronectin matrix assembly. Am J Respir Cell Mol Biol , 538–45.

Rongish, B., Drake, C., Argraves, W., Little, C., 1998. Identification of the developmental marker, JB3-antigen, as fibrillin-2 and its de novo organization into embryonic microfibrous arrays. Dev. Dyn. 212, 461–71.

Rudnick, D., 1933. Developmental capacities of the chick lung in chorioallantoic grafts. J. Expt. Zool. 66, 125–154.

Sakai, L., Keene, D., Engvall, E., 1986. Fibrillin, a new 350-kD glycoprotein, is a component of extracellular microfibrils. J Cell Biol. 103, 2499–509.

Schoenwolf, G., Garcia-Martinez, V., Dias, M., 1992. Mesoderm movement and fate during avian gastrulation and neurulation. Dev. Dyn. 193, 235–248.

Sepich, D. S., Calmelet, C., Kiskowski, M., Solnica-Krezel, L., 2005. Initiation of convergence and extension movements of lateral mesoderm during zebrafish gastrulation. Dev Dyn. 234, 279–92.

Sherratt, M. J., Baldock, C., Haston, J. L., Holmes, D. F., Jones, C. J. P., Shuttleworth, C. A., Wess, T. J., Kielty, C. M., 2003. Fibrillin microfibrils are stiff reinforcing fibres in compliant tissues. J Mol Biol 332, 183–93.

Sivakumar, P., Czirok, A., Rongish, B., Divakara, V., Wang, Y. P., Dallas, S., 2006. New insights into extracellular matrix assembly and reorganization from dynamic imaging of extracellular matrix proteins in living osteoblasts. J Cell Science xxx, xxx–xx.

Skoglund, P., 1996. The role of Xenopus fibrillin in the early embryo: clues from a dominant negative approach. Ph.D. thesis, UCSD, San Diego.

Sottile, J., Hocking, D. C., 2002. Fibronectin polymerization regulates the composition and stability of extracellular matrix fibrils and cell-matrix adhesions. Mol Biol Cell 13, 3546–59.

Stoplak, D., Harris, A., 1982. Connective tissue morphogenesis by fibroblast traction. Dev. Biol. 90, 383 – 398.

Timpl, R., Sasaki, T., Kostka, G., Chu, M.-L., 2003. Fibulins: a versatile family of extracellular matrix proteins. Nat Rev Mol Cell Biol , 479–89.

Tomasek, J. J., Hay, E. D., Fujiwara, K., 1982. Collagen modulates cell shape and cytoskeleton of embryonic corneal and fibroma fibroblasts: distribution of actin, alpha-actinin, and myosin. Dev Biol 92, 107–22.

Trinkaus, J., 1984. Cells into Organs. The forces that shape the embryo. Prentice-Hall, Inc., Englewood Cliffs, New Jersey, 2nd edn.

Velling, T., Risteli, J., Wennerberg, K., Mosher, D. F., Johansson, S., 2002. Polymerization of type i and iii collagens is dependent on fibronectin and enhanced by integrins alpha 11beta 1 and alpha 2beta 1. J Biol Chem 277, 37377–81.

Vernon, R., Lara, S., Drake, C., Iruela-Arispe, M., Angello, J., Little, C., Wight, T., Sage, E., 1995. Organized type I collagen influences endothelial patterns during “spontaneous angiogenesis in vitro”: planar cultures as models of vascular development. In Vitro Cell Dev Biol Anim 31(3), 120 – 131.

Visconti, R., Barth, J., Keeley, F., Little, C., 2003. Elastin and related fibrillar proteins in early development. Matrix Biol. 22, 109–21.

Winklbauer, R., Keller, R. E., 1996. Fibronectin, mesoderm migration, and gastrulation in xenopus. Dev Biol 177, 413–26.

Wolf, K., Friedl, P., 2005. Functional imaging of pericellular proteolysis in cancer cell invasion. Biochimie 87, 315–20.

Wu, Y. J., La Pierre, D. P., Wu, J., Yee, A. J., Yang, B. B., 2005. The interaction of versican with its binding partners. Cell Res 15, 483–94.

Wunsch, A., Little, C., Markwald, R., 1994. Cardiac endothelial heterogeneity defines valvular development as demonstrated by the diverse expression of JB3, an antigen of the endocardial cushion tissue. Dev. Biol. 165, 585–601.

Yang, X., Dormann, D., Munsterberg, A. E., Weijer, C. J., 2002. Cell movement patterns during gastrulation in the chick are controlled by positive and negative chemotaxis mediated by fgf4 and fgf8. Dev. Cell 3, 425–37.

Zamir, E., Katz, B. Z., Aota, S., Yamada, K. M., Geiger, B., Kam, Z., 1999. Molecular diversity of cell-matrix adhesions. J Cell Sci 112 (Pt 11), 1655–69.

Zamir, E. A., Czirok, A., Rongish, B. J., Little, C. D., 2005. A digital image-based method for computational tissue fate mapping during early avian morphogenesis. Ann Biomed Eng 33, 854–65.

Zhang, H., Apfelroth, S., Hu, W., Davis, E., Sanguineti, C., Bonadio, J., Mecham, R., Ramirez, F., 1994. Structure and expression of fibrillin-2, a novel microfibrillar component preferentially located in elastic matrices. J Cell Biol. 124(5), 855–63.

Zhong, C., Chrzanowska-Wodnicka, M., Brown, J., Shaub, A., Belkin, A. M., Burridge, K., 1998. Rho-mediated contractility exposes a cryptic site in fibronectin and induces fibronectin matrix assembly. J Cell Biol 141, 539–51.

Figure captions

FIGURE 1 The localization of fibronectin (red) and fibrillin-2 (green) in a gastrulation/neurulation stage avian embryo. The en face views (a-d,g,h) and optical transverse sections (e,f) show the ECM molecules labeled by whole mount JB3 (anti fibrillin-2) and B3D6 (anti fibronectin) immunostaining in a HH stage 6 (Hamburger and Hamilton, 1951) quail embryo. a: Wide-field epifluorescence microscopy reveals a similar general pattern of distribution of both fibronectin and fibrillin-2 in the caudal half of the embryo. Fibrillin-2 connects the somites (cyan arrow), and forms long filaments in the pre-somitic mesoderm which become more pronounced in time (Fig. 2). Regions analogous to A and B are further analyzed by laser scanning optical microscopy (b-h). Panels b, c and d show 2.2μm thick optical sections of boxed area A at the ventral surface, middle and dorsal surface of the mesoderm, respectively. e: A digitally reconstructed transverse section along the white lines in (b-d) shows fibronectin and fibrillin filaments spanning the mesoderm (white arrowheads). f: Anterio-posterior projection of all transverse sections similar to (e) reveal ECM accumulation at the dorsal and ventral surfaces of the mesodermal germ layer. Digitally reconstructed oblique projections of boxed area B (g, h) demonstrate co-localization of filaments (yellow) as well as filaments extending in the dorsal-ventral direction (white brackets). g: En face view, rotated by 10^o along the lateral (x) axis. h: Oblique view, rotated by 50^o along the lateral (x) axis. H: Hensen's node, n: notochord, s: primitive streak, d: dorsal, v: ventral

FIGURE 2 Fibrillin-2 reorganization coincident with somitogenesis. Selected filaments, marked with the colored circles, visibly alter their relationship with nearby filaments and the axis. Despite this motion, the filaments retain connectedness and shape to some degree. Blue boxes denote formed somites. n: notochord. Reprinted from (Czirok et al., 2004).

FIGURE 3 Detailed view of ECM filament motion. a: The displacements of fibrillin-2 filaments during a 20 minute interval are depicted within a region analogous to boxed area A of Fig. 1, and in a region containing somites (inset). The earlier and latter immunofluorescence pattern is presented in the green and blue channels, respectively. Co-localization of the two channels (cyan) indicates absence of motion (inset). Yellow arrows represent filament displacements, as obtained by manual tracking. The change in filament configuration, as indicated by the similar length of the white brackets, is small compared to the displacements. b: ECM filament motion, estimated by particle image velocimetry (Zamir et al., 2005). Yellow arrows represent manual tracking results from panel (a). Red arrows represent the results of a two-step predictor-corrector PIV algorithm with 64 and 16 pixel windows, without data smoothing in the corrector step. Blue arrows represent the estimated tissue motion component, determined by the same algorithm with 128 and 64 pixel windows and an additional thin plate spline smoothing.

FIGURE 4 Comparison of fibronectin (red) and fibrillin-2 (green) rearrangements. Immunolabeled ECM components are depicted at two time points, separated by 20 minutes (a,b). Despite the general displacement shown in Fig. 3, the relative configurations of fibronectin and fibrillin-2 filaments remained mostly unchanged (magenta circles). However, at certain positions the relative motion of the two ECM components is evident (cyan circles), a difference attributed to local cell activity. c: Temporal changes in fluorescence intensities along the white line in panels a and b. The continuous curves represent filament trajectories. Within the cyan circle, a fibronectin filament is seen relocating between two fibrillin-2 filaments. In contrast, the two ECM components move as a single composite structure within the magenta circle. d: The local component of the displacement field, calculated by PIV. The endpoint of the displacement vector is indicated by a

circle (fibronectin: red, fibrillin-2: green).

FIGURE 5 Quantitative analysis of the tissue and local motion components. a: Distribution of the magnitude of the tissue (solid line) and local (dashed line) motion components, calculated for fibronectin throughout the caudal embryo. The average magnitudes are markedly different: 4 μm and 1.2 μm for the tissue and the local components, respectively. b: Distribution of the difference between fibronectin and fibrillin-2 displacements. The magnitude of the difference between the displacement vectors obtained for the two ECM components is calculated throughout the caudal embryo for each motion component (tissue motion: solid line, local rearrangements: dashed line). Compared to the typical magnitude of the tissue displacement, the tissue components are essentially the same for both fibronectin and fibrillin-2 (average difference is 0.15 μm, 3% of the average magnitude). In contrast, the difference in the local component (average is 0.8 μm) is five-fold larger, and is comparable with 1.2 μm, the typical magnitude of the local displacement vectors. Displacements were calculated from 40 images, each taken 5 minutes apart.

FIGURE 6 Tissue component of ECM displacements. Displacement vectors (circles at endpoints), were obtained by PIV and are averaged for each grid point over 10 frames (40 minutes). The motion pattern obtained from a two-somite embryo (a) and 3 hours later from the same, four-somite embryo (b) are very similar, essentially consisting of two vortices, on each side of the embryonic axis. Centers of rotation are marked by asterisks. The gray lines denote the somites, notochord, Hensen's node and the primitive streak (from top to bottom).

FIGURE 7 Analysis of the tissue component of ECM motion. a: The divergence of the displacement field shows condensation of labeled ECM filaments around the site of somitogenesis

(blue) and dilution at the caudal end of the primitive streak (yellow). b: The motion also deforms the ECM. Tissue deformation is indicated by two-headed arrows: The size of the symbols is proportional to the magnitude of the deformation, and the lines are parallel to the direction of stretch. The gray lines denote the somites, notochord, Hensen's node and the primitive streak (from top to bottom).

FIGURE 8 Magnitude of the local component of ECM rearrangements, averaged over 10 consecutive frames (40 minutes). Hensen's node and the area surrounding the primitive streak displays especially active local ECM rearrangements (red). The numeric values are given in units of μm/h. The gray lines denote the somites, notochord, Hensen's node and the primitive streak (from top to bottom).

FIGURE 9 Hierarchical assembly of ECM filaments. An image sequence depicting an area located lateral to the streak (comparable to boxed region B in Fig. 1) as it moves with the tissue. White circles label individual globules of ECM material, which typically contain both fibronectin and fibrillin-2. In the course of three hours, the globules assume an ordered, linear shape, which remains stable until the end of observation, 7 hours later (not shown). Brackets indicate areas where previously distinct ECM objects merge (assume a stable linear arrangement). As an example, the filament marked by the cyan ellipse in panel (b) is created from the material enclosed in the cyan ellipse in panel (a). Both areas are shown with greater detail in the insets. During the assembly process, the original punctate immunofluorescence gives rise gradually to a filamentous pattern.

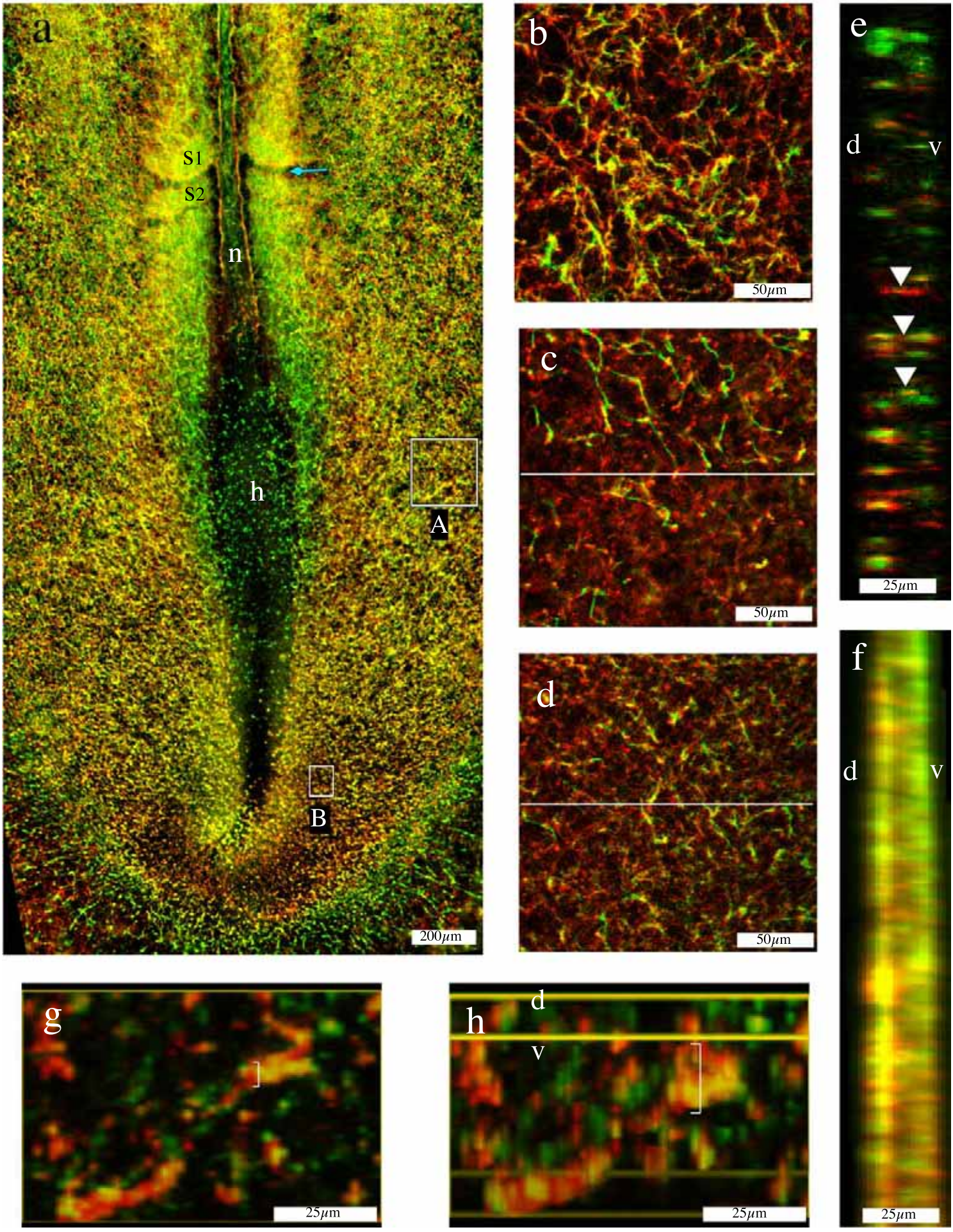
a
S1
S2
n
h
A
B
200μm
b
50μm
c
50μm
d
50μm
e
d
v
25μm
f
d
v
25μm
g
25μm
h
d
v
25μm

Fig. 1

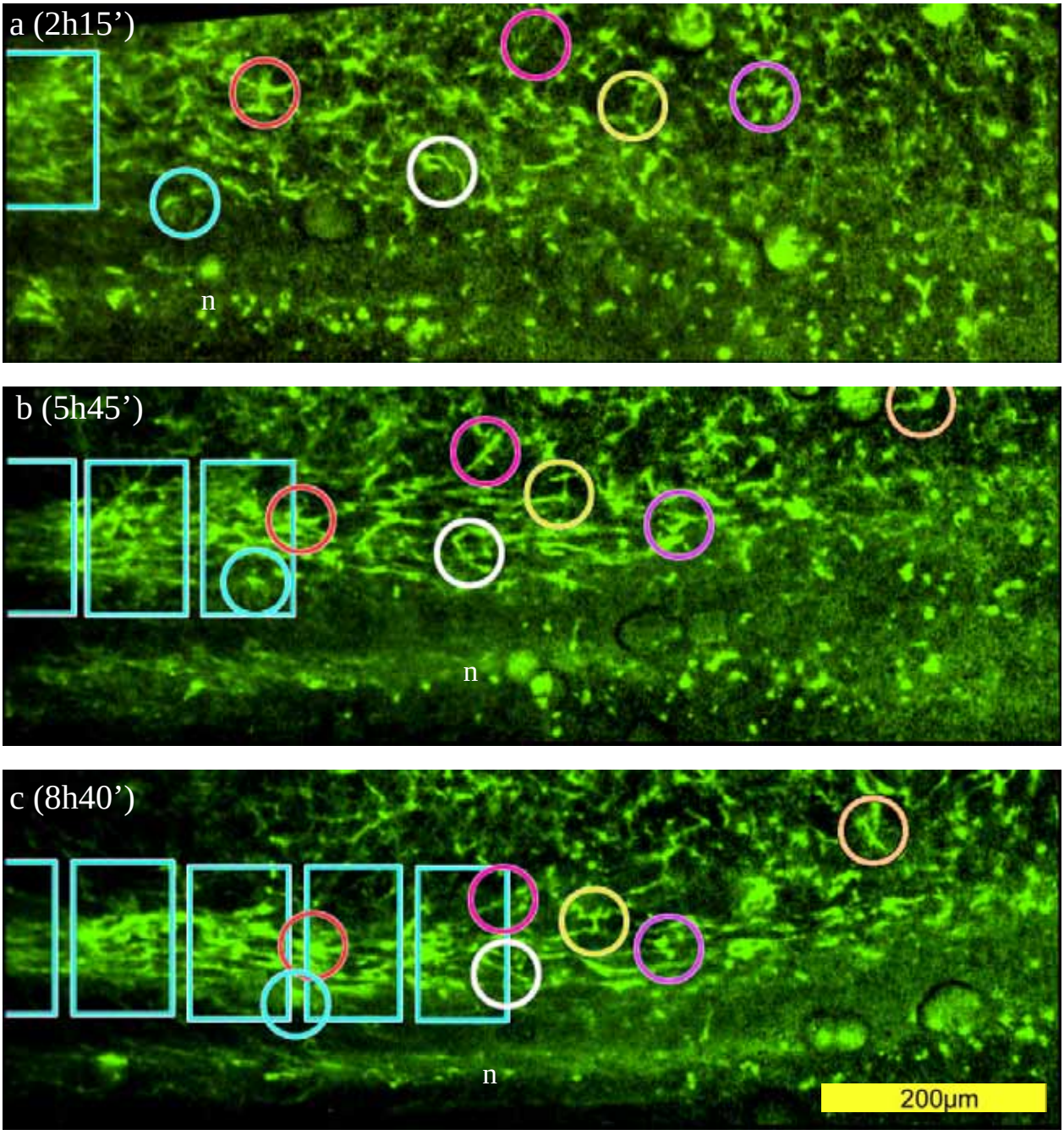

Fig. 2

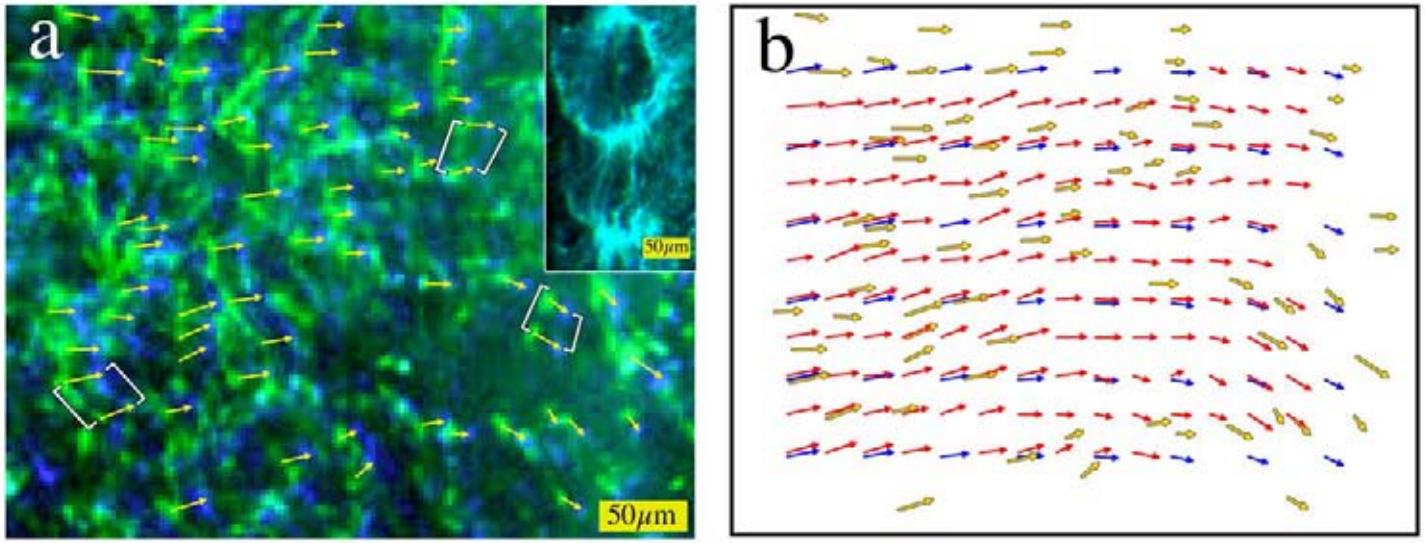

Fig. 3

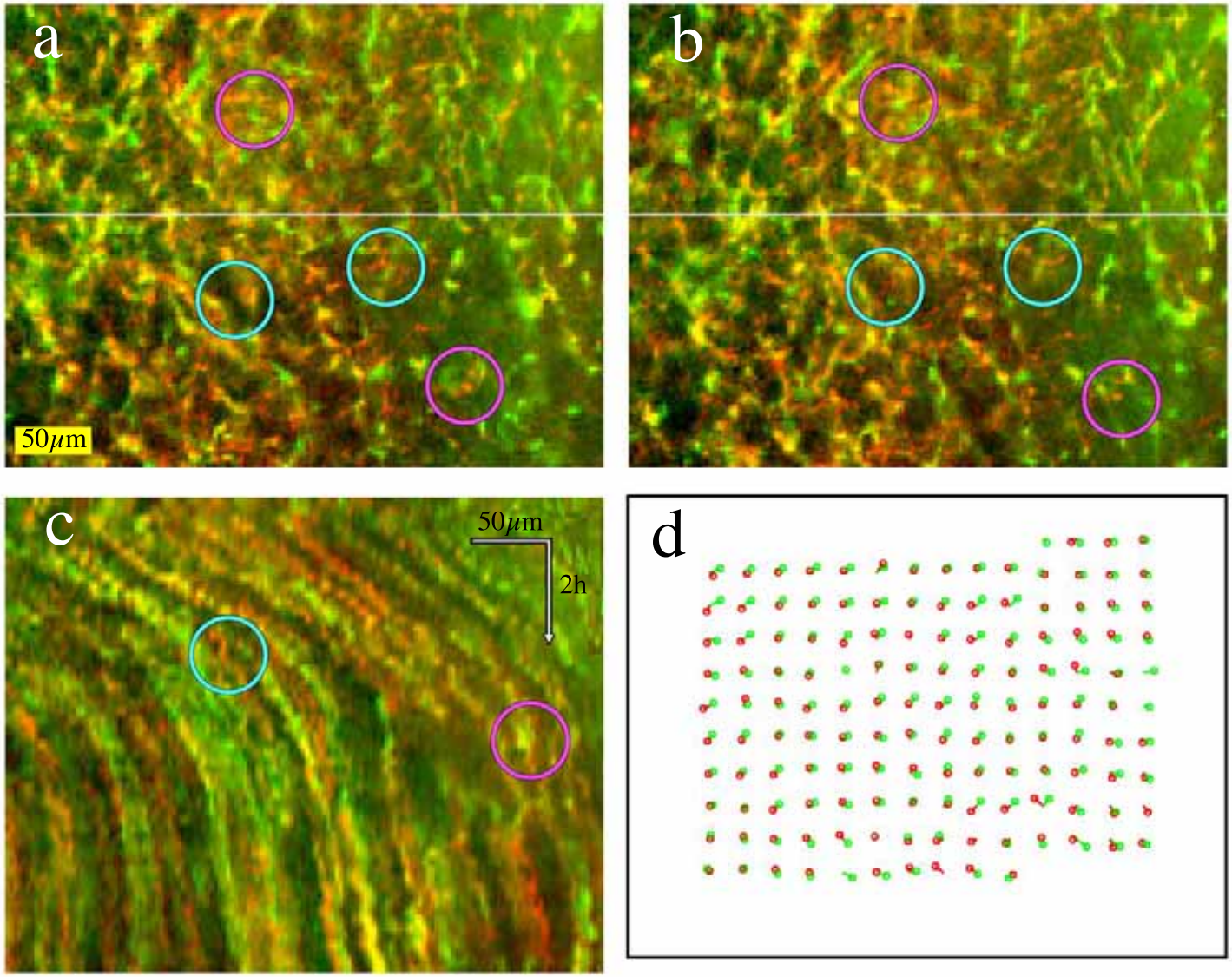

Fig. 4 □

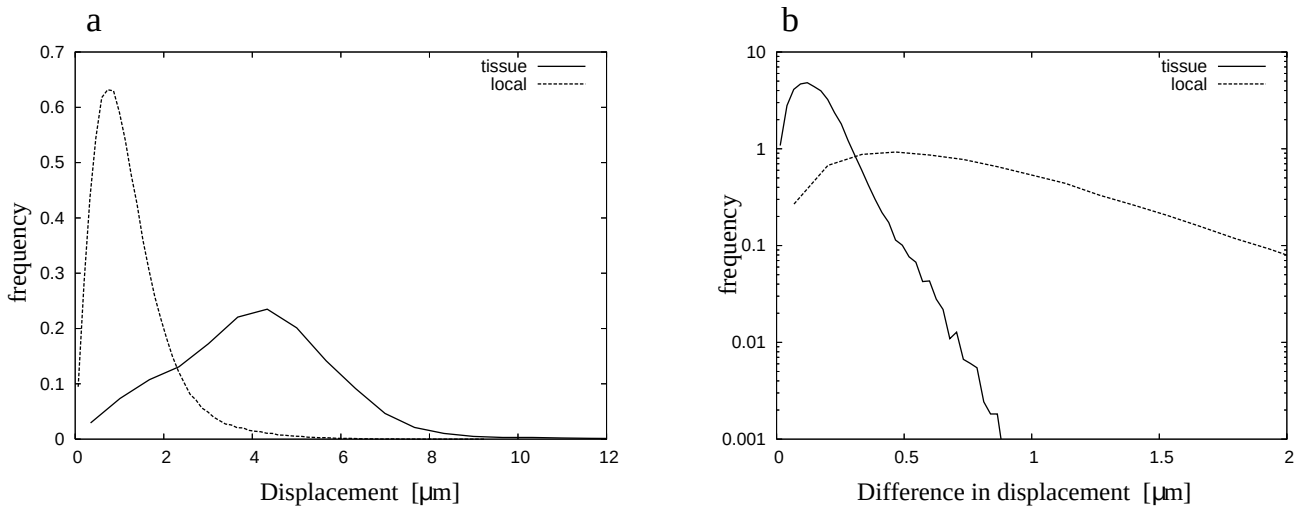
a
b
tissue
local
frequency
Displacement [μm]
Difference in displacement [μm]
0
0.1
0.2
0.3
0.4
0.5
0.6
0.7
2
4
6
8
10
12
0.001
0.01
1
0.5
1.5

Fig. 5

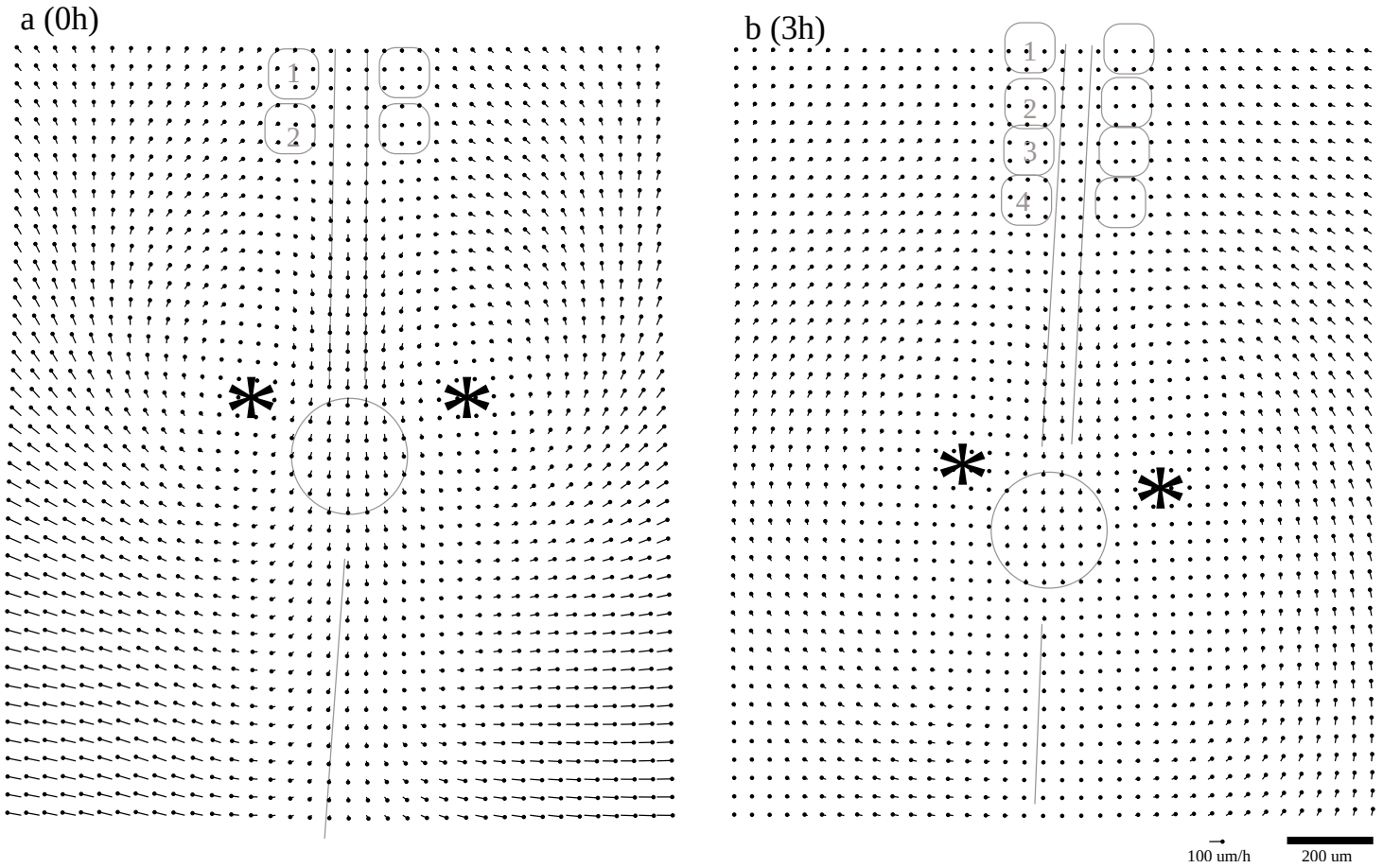

Fig. 6□

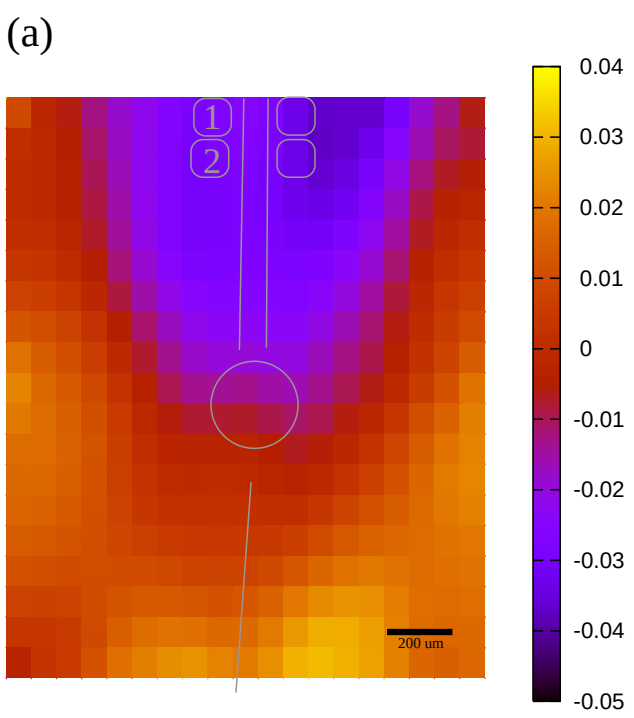

Fig. 7□

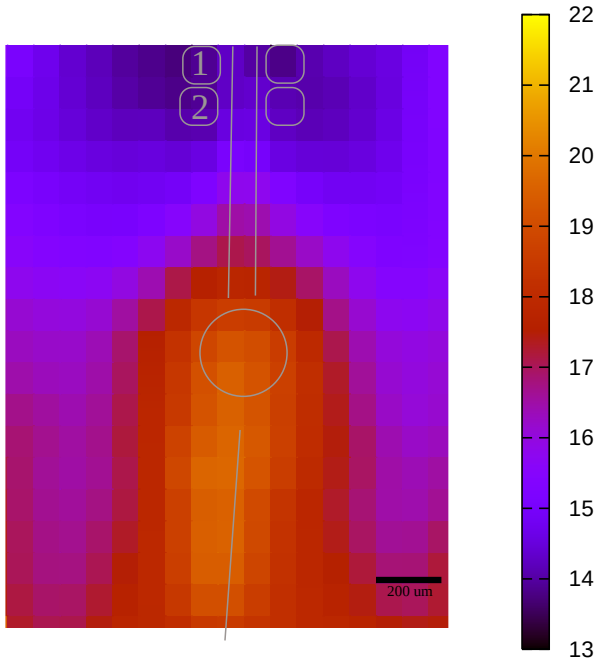

Fig. 8

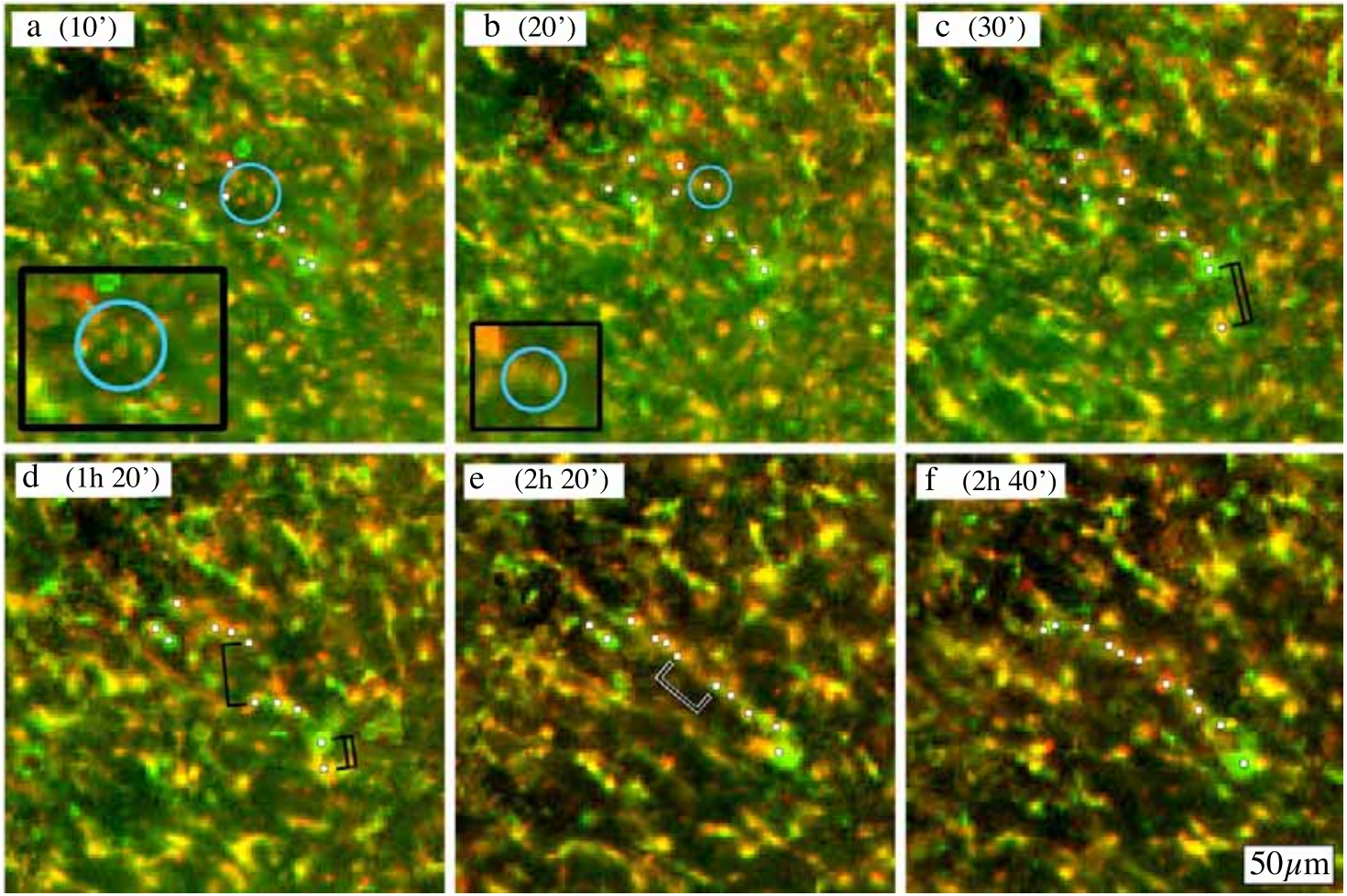

Fig. 9